Supplemental data to the manuscript

Pals1 haplo-insufficiency results in proteinuria and cyst formation.

By

Thomas Weide[1*§], Beate Vollenbröker[1*], Ulf Schulze[1], Ivona Djuric[1], Maria Edeling[1],

Jakob Bonse[1], Florian Hochapfel[2], Olga Panichkina[2],

Dirk-Oliver Wennmann[1], Britta George[1], Seonhee Kim[3], Christoph Daniel[4], Jochen Seggewiß[5]

Kerstin Amann[4], Wilhelm Kriz[6], Michael P. Krahn[2],

and

Hermann Pavenstädt[1§]

[1)] Internal Medicine D, University Hospital of Münster, Germany

[2)] Institute for Molecular and Cellular Anatomy, University of Regensburg, Regensburg, Germany

[3)] Shriners Hospitals Pediatric Research Center, Department of Anatomy and Cell Biology, Lewis Katz School of Medicine, Temple University, Philadelphia, PA, 19140, USA

[4)] Nephropathology Department, Institute of Pathology, Erlangen-Nürnberg University, Erlangen, Germany

[5)] Interdisciplinary Center for Clinical Research, University of Münster, Muenster, Germany

[6)] Department of Neuroanatomy, Medical Faculty Mannheim, University of Heidelberg, Mannheim, Germany

[*)] TW and BV contributed equally to this work

[§] Correspondence to:
Hermann Pavenstädt, Tel. + 49 251 83 47517; Fax + 49 251 83 57943;
Email: hermann.pavenstaedt@ukmuenster.de or

Thomas Weide, Tel. + 49 251 83 57939; Fax + 49 251 83 57943,
Email : weidet@uni-muenster.de

Internal Medicine D, University Hospital of Münster, Albert-Schweitzer-Campus 1, 48149 Münster, Germany

Supplemental data:

Supplemental Figures and Tables

Fig. SF1: Pals1 expression during nephrogenesis is crucial for formation of a functional renal filtration barrier.

Fig. SF2: Pals1 is expressed in the nephron.

Fig. SF3: In cyst-lining cells of ADPKD biopsies, Pals1 polarization is only occasionally perturbed.

Fig. SF4: Analysis of tubular cyst development

Fig. SF5: Relative expression levels of target genes of the Hippo pathway and apical polarity genes.

Fig. SF6: Taz Antibody is suitable for immunohistology staining

Fig. SF7: In Pals1 KD MDCK cells, nuclear export of Yap is delayed.

Fig. SF8: Reduced Pals1 expression in Hek293T cells results in altered Hippo signaling.

Fig. SF9: Gene expression analysis in Pals1-depleted mice versus littermate controls.

Table ST1: Reduced Pals1 expression results in an increased expression of renal injury marker genes.

Table ST2: Extended methods: details of antibodies and primer.

Additional supplemental data files:

Suppl. data file 1 / SD1 (Excel file): Gene microarray: GEO accession number: GSE77628

Suppl. data file 2 / SD2 (Excel file): Evaluation of Gene microarray data.

Suppl. Fig. SF1

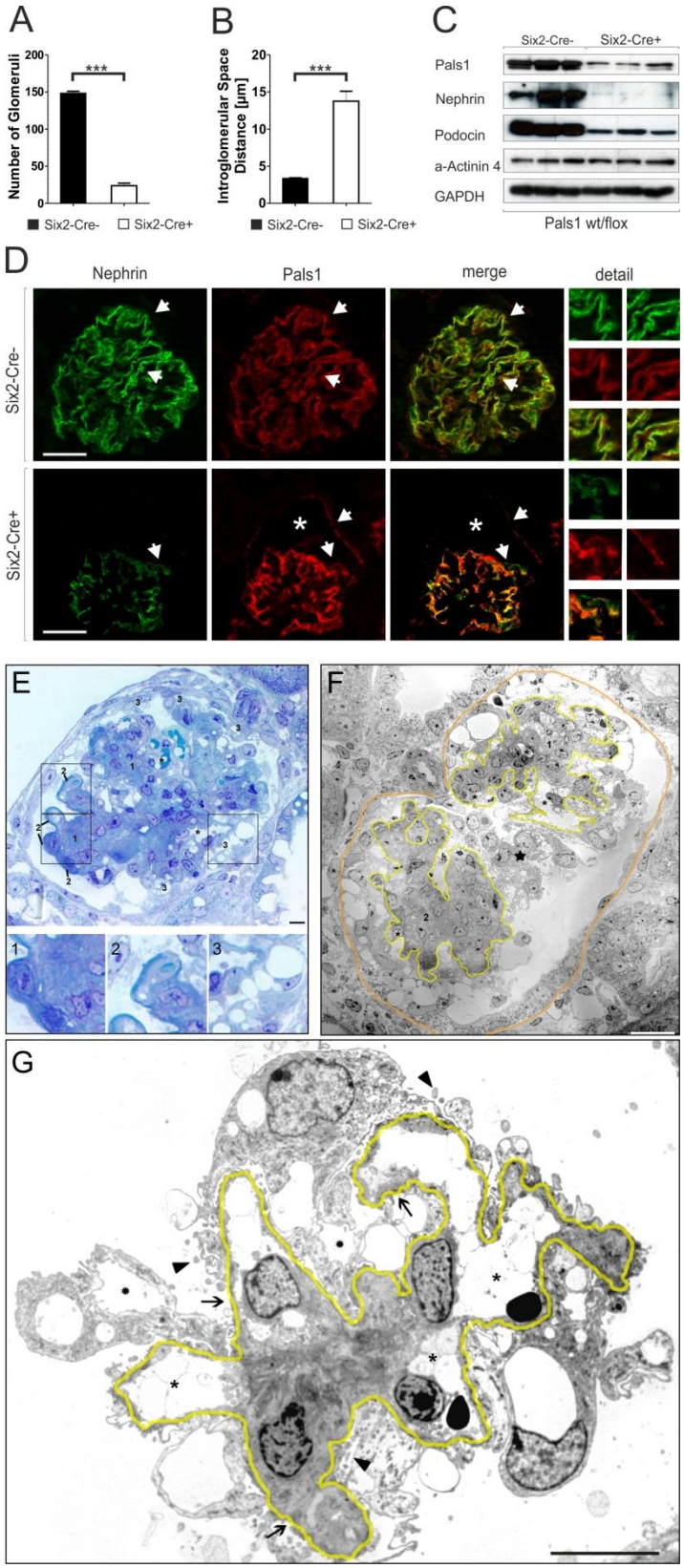

Fig. SF1: *Pals1 expression during nephrogenesis is crucial for formation of a functional renal filtration barrier.*

Analysis of the glomerular phenotype of the Six2-Cre; Pals1$^{wt/fl}$ (Six2-Cre+) mutant at 4 weeks of age in comparison with the Pals1$^{wt/fl}$ (Six2-Cre-) control. **A:** Distribution of glomerular numbers in Six2-Cre+ and Six2-Cre- mice. **B:** Distribution of intraglomerular distances (glomerulocyst formation) in Pals1-depleted (Six2-Cre+) and control versus (Six2-Cre-) kidneys. **C:** Western blot analysis of expression of Pals1, the slit-diaphragm-specific proteins nephrin and podocin, and α-actinin 4 and GAPDH (loading controls) in independent samples from three Six2-Cre+ and three Six2-Cre- mice. **D:** IF analysis of glomeruli derived from Six2-Cre+ and Six2-Cre- mice stained for Pals1 (red) and nephrin (green). Arrows mark areas shown in detail on the right, asterisks mark the glomerulocyst in the Six2-Cre+ glomerulus. Scale bar: 20 µm. **E:** Advanced stage of glomerular degeneration: Glomerular profile with massive expansion of the mesangio-capillary area (1), but with only a few clearly defined capillaries (asterisks). Podocytes have lost contact with the GBM over wide areas, leaving behind extensive bare tracts of GBM (2). At other sites (3), detaching podocytes with many pseudocysts have assembled into clusters that form bridges between the tuft and Bowman‘s capsule. LM, Scale bar: 5 µm. **F:** Advanced stage of glomerular degeneration: The glomerular basement membrane (GBM) is outlined in yellow, the parietal basement membrane (PBM) in orange. Glomerular profile containing two lobules (1 and 2) with podocytes that are in the process of detaching or have already detached from the GBM. The mesangio-capillary area (enclosed by the GBM) is massively expanded but contains only very few obvious capillaries (star). The detaching podocytes form a cell cluster floating within Bowman‘s space (star). The lower-left side of lobule 2 is covered by a huge crescent consisting of fully or partially detached podocytes that connect the tuft to Bowman‘s capsule. A similar but smaller crescent is seen at the upper side of lobule 1; TEM. Scale bar: 20 µm. **G:** Comparatively early stage of glomerular degeneration: Glomerular lobule with podocytes that are severely damaged, characterized by widespread loss of foot processes, pseudocysts (stars) and cytoplasm shedding (arrowheads). Bare areas of GBM are seen at a few sites (arrows). Major damage is also seen in the GBM (outlined in yellow). Empty spaces in the mesagium (asterisks) seem to coalesce with remnants of capillaries that contain a trapped erythrocyte at two sites. TEM. Scale bar: 10 µm.

Methods

For TEM analysis small cortical tissue blocks were fixed overnight in Sörensen's buffer containing 2.5% glutaraldehyde. Blocks were then treated with 4% OsO_4 and embedded in Epon. Thin sections (1 µm) were stained with methylene blue and studied by light microscopy. Ultrathin sections were stained with uranyl acetate and studied by transmission electron microscopy[1].

Pals1 expression is crucial for the function of the renal filtration barrier. Numbers of glomeruli were reduced in 4-week-old Six2-Cre; $Pals1^{wt/fl}$ mice (Fig. SF1A). Furthermore, in these mice the average distance between the glomerulus and Bowman´s capsule was much larger than in control littermates (Fig. SF1B). In contrast to α-actinin 4 and GAPDH, expression of the slit-diaphragm proteins nephrin and podocin was strongly reduced in Pals1-deficient kidneys (Fig. SF1C). In addition, the nephrin-like distribution of Pals1 (Fig. SF1D, upper panel) was clearly altered in injured glomeruli (Fig. SF1D, lower panel).

Examination of Six2-Cre; $Pals1^{wt/fl}$ kidneys by light microscopy (Fig. SF1E) and transmission electron microscopy revealed advanced stages of glomerular injury (Fig. SF1F, G) and an expansion of the mesangio-capillary area, with podocyte detachment from the glomerular basement membrane leaving large areas of the GBM bare. In some areas detached podocytes assembled into clusters that formed crescent-like bridges between the tuft and Bowman's capsule. In early stages of glomerular degeneration podocytes exhibiting widespread foot-process loss and cytoplasm shedding were observed (Fig. SF1G).

Suppl. Fig. SF2:

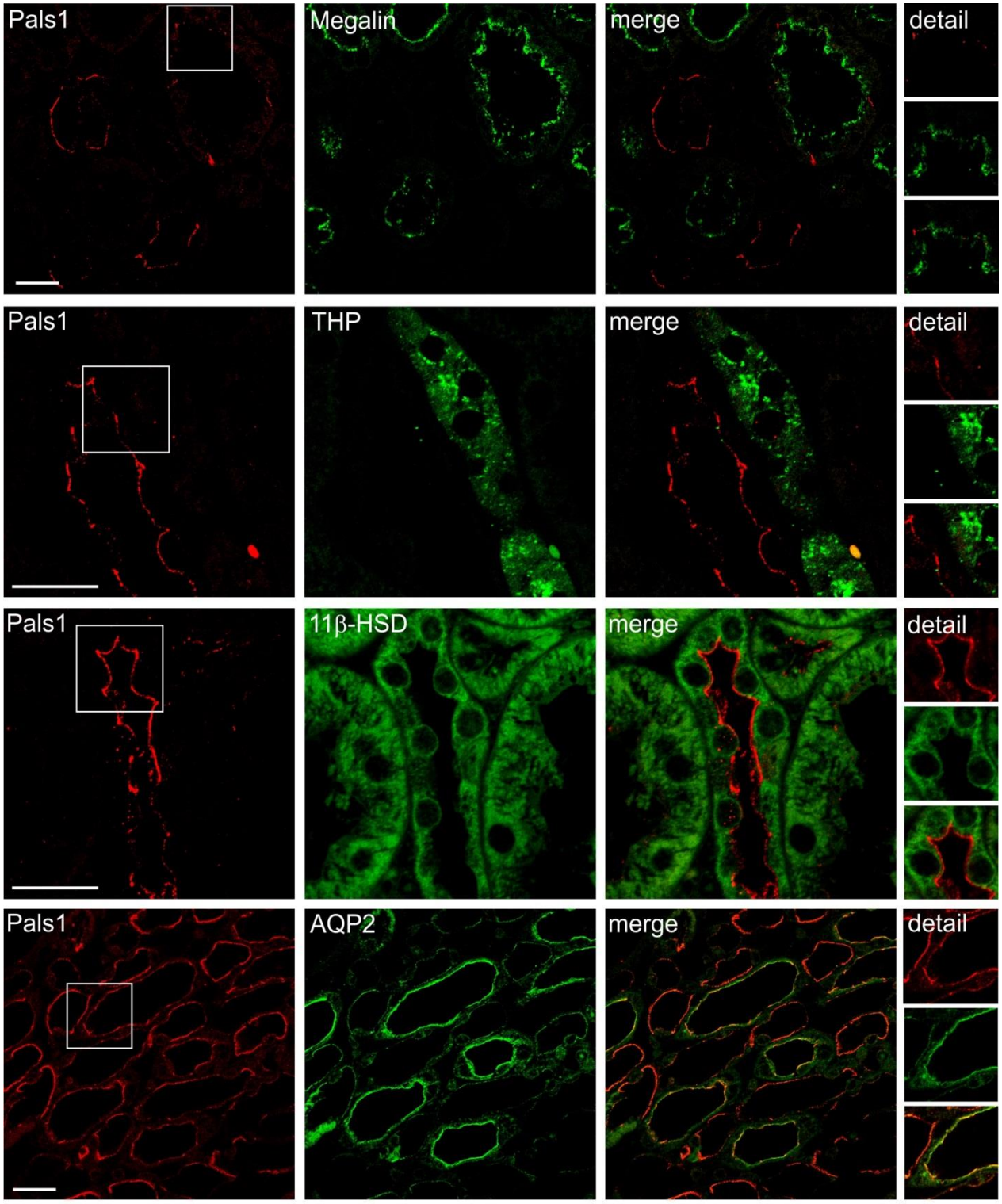

Fig. SF2: *Pals1 is expressed in the nephron.*

Immunofluorescence staining of Pals1 and co-staining with diverse tubulus markers in wildtype mice (6 months). Co-staining of Pals1 with Megalin (proximal tubule marker, **A**), Tamm-Horsfall Protein (thick ascending limb of the loop of Henle, **B**), 11β-HSD (distal tubules, **C**) and AQP2 (collecting duct, **D**). Scale bar: 50 µm.

Suppl. Fig. SF3

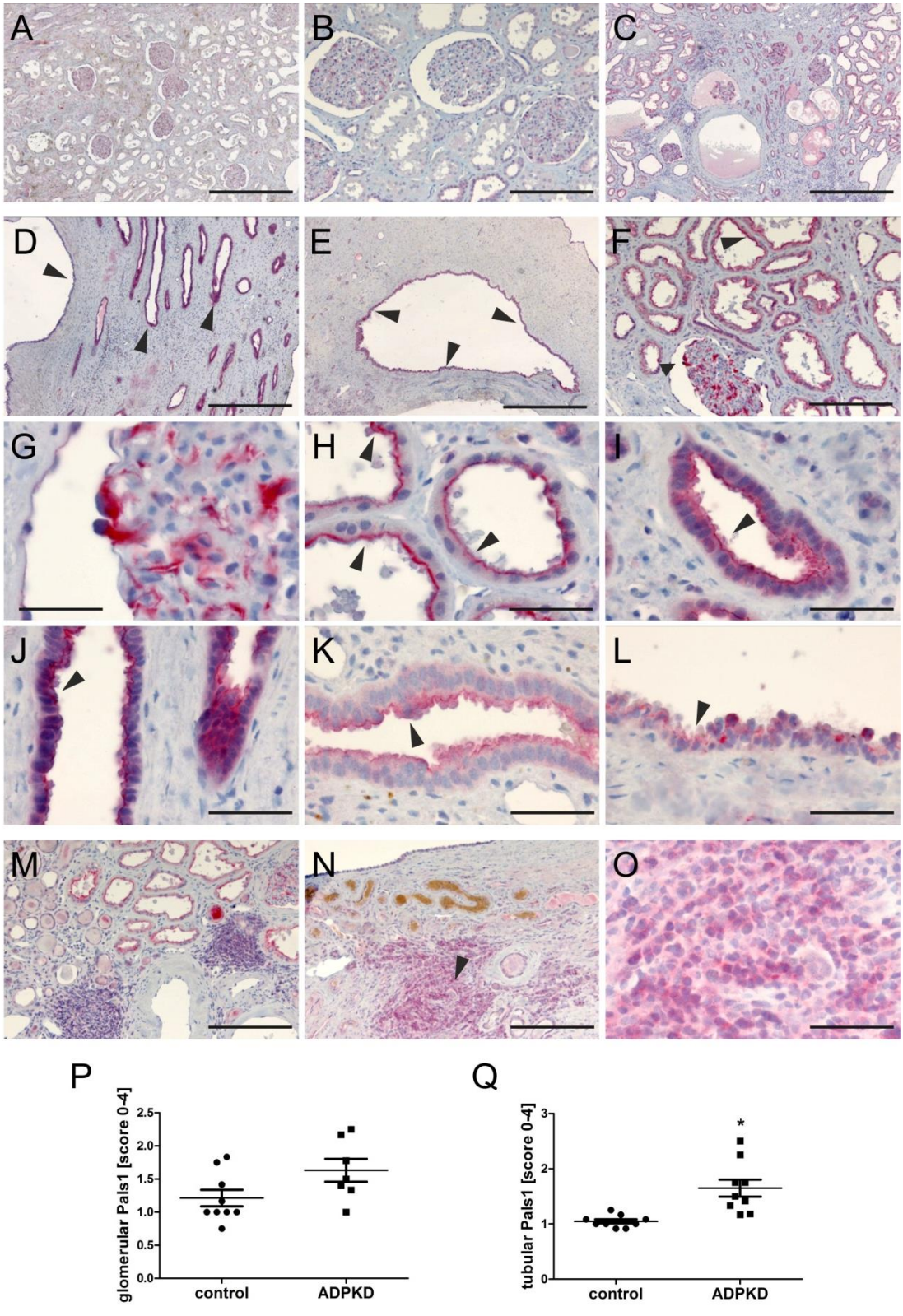

Fig. SF3: *In cyst-lining cells of ADPKD biopsies, Pals1 polarization is only occasionally perturbed*.

A, B: Overview of Pals1 staining (red) in tumor-free kidney controls shows Pals1-positive staining in glomeruli and tubular cells. Scale bars: 500 µm (**A)** and 200 µm (B). **C-E:** Overview of Pals1 staining (red) in biopsies from ADPKD patients showed Pals1-positive staining in glomeruli (g) and tubular cells and cyst-lining cells (arrowheads, **D-E**). Scale bar: 500 µm (**C-E**). **F-J:** In ADPKD patients Pals1 is expressed in glomerular podocytes (**F**, scale bar: 200 µm, detail in **G**, scale bar: 30 µm), and predominantly in the apical membrane of dilated cystic tubuli (**H, J,** arrowheads, Scale bars: 50 µm). In addition, low levels of Pals1 are detectable in the cytoplasm of dilated cystic tubular cells (**I, J**). **K-L:** The overall impression is that Pals1 is strongly found in the apical membrane of cyst lining cells. However, In some cyst lining-cells, Pals1 staining is diffuse and not strongly polarized apically (scale bar: 50 µm). Thus, in ADPKD it seems that the hyperproliferative cysts show more diffuse staining. **M-O:** Diffuse Pals1 staining is detectable in infiltrating cells of ADPKD biopsies. The region marked by the arrowhead in **N** is shown at higher magnification in **O**. Scale bars: 200 µm (**M, N**) and 50 µm (**O**). **P:** Semi-quantitative evaluation of glomerular Pals1 staining in ADPKD compared to tumor-free controls. **Q:** Semi-quantitative evaluation of tubular Pals1 staining in ADPKD compared to tumor-free controls; *p<0.002.

Methods

Source of human renal tissue

Archival tissues from core needle biopsies performed between 2003 and 2012 at the Department of Nephropathology (Erlangen, Germany) were used for this study (n = 28). The morphological diagnosis of focal segmental glomerulosclerosis (FSGS; n=10) was made by the local pathologist. In addition, Pals1 expression was evaluated in 9 biopsies from patients with autosomal dominant polycystic renal disease (ADPKD). Control tissues without evidence of renal disease (n = 9) were obtained from distant portions of kidneys that were surgically excised because of the presence of a localized neoplasm. The use of tissue specimens was approved by the Ethics Committee of the Medical Faculty of the University of Erlangen.

Evaluation of Pals1/MPP5 expression in human renal biopsies

To determine the localization and expression level of MPP5 in the healthy and diseased kidney immunostaining of paraformaldehyde-fixed, paraffin-embedded biopsies was performed. A rabbit anti-Pals1/Mpp5 purchased from Sigma-Aldrich (HPA000993) was used as the primary antibody. After deparaffination, rehydration and blocking of endogenous peroxidase, antigens were retrieved in target retrieval solution (DAKO diagnostics, Hamburg, Germany) by heating for 1 minute in a pressure cooker. Bound anti-MPP5 antibody was detected by incubation with biotinylated donkey anti-rabbit antibody and horseradish-conjugated avidin (ZytoChem-Plus AP Polymer kit, Zytomed Systems GmbH, Berlin, Germany) following the manufacturer's instructions and using Fast red as substrate. Negative controls for immunostaining included either omission of the primary antibody or its substitution with equivalent concentrations of an irrelevant pre-immune rabbit IgG.

Suppl. Fig. SF4

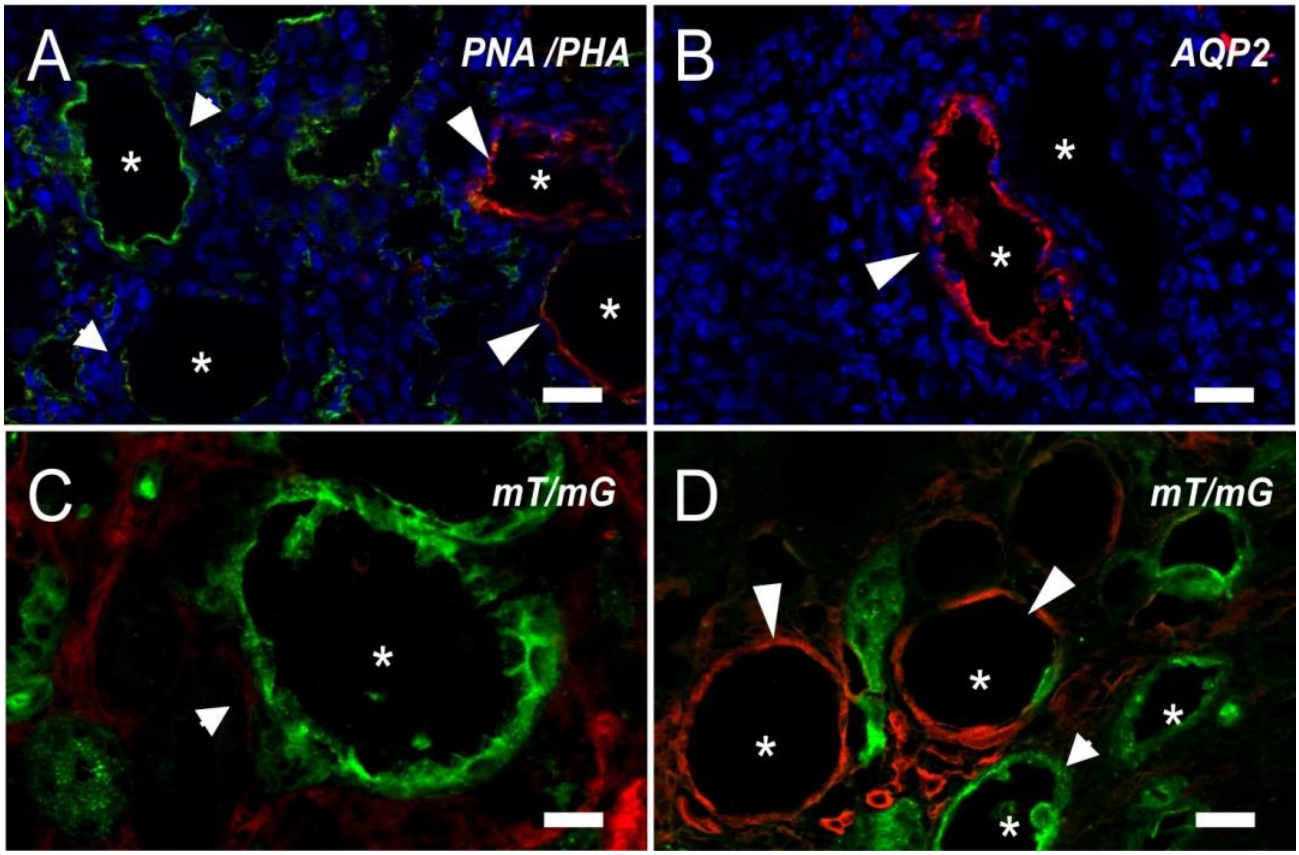

Fig. SF4: *Analysis of tubular cyst development*

A-D: Cysts in Pals1depleted kidneys (Six2-Cre+) were positive for proximal (PNA, red) and distal (PHA, green) tubular markers (**A**). Some cysts were positive for the collecting duct marker AQP2 (**B**). **C, D:** Crossing of Six2-Cre+ mice (Pals1$^{wt/flox}$ x Six2-Cre+) with the double fluorescence mTomato/mGFP reporter line allows one to visualize Cre-positive cells (green) in Pals1-deficient kidneys. Cysts showed a green (Cre+) (**C**), red (Cre-) or a mixed green-red (**D**) fluorescence, indicating secondary cyst formation in tubular regions that retain both Pals1 alleles. Asterisks mark cysts, arrowheads cyst-lining regions; Scale bars: 20 µm.

Characterization of cyst origin:

The different sizes and morphologies (Fig. 3B, b1-b3) suggested that cysts developed from various sections of the nephron. We addressed this by staining with the lectins PHA (phytoheme agglutinin) and PNA (peanut agglutinin), which specifically mark regions of the proximal and distal tubular parts of the nephron, respectively. Most cysts could be labeled with PHA or PLA (Fig. SF3A). However, some cysts were positive for the collecting duct marker Aquaporin 2 (Fig. SF3B). Since Six2-positive cells are progenitors of proximal and distal tubules, but not of the collecting duct, this result argued for progressive cyst formation in nephron sections of non-cap-mesenchymal origin.

To further address this issue, we made use of a genetic approach. Crossing the Six2-Cre driver with mT/mG reporter mice results in a Cre-dependent fluorescence switch from red (mTomato) to green (mGFP) fluorescence in all Cre-expressing cells[2,3]. Therefore, we generated Six2-Cre; mT/mG mice and crossed them with homozygous conditional Pals1 knockout mice to obtain triple transgenic Six2-Cre; mT/mG x Pals1$^{wt/fl}$ progeny. These animals developed a strong kidney phenotype similar to that seen in Six2-Cre; Pals1$^{wt/fl}$ mice (not shown). As expected, most of the cyst-lining cells showed green fluorescence (Fig. SF3C). However, some cysts displayed a red or a mixed green-red fluorescence (Fig. SF3D), confirming the occurrence of secondary cyst formation in tubular regions that carry two wild-type Pals1 alleles.

Suppl. Fig. SF5

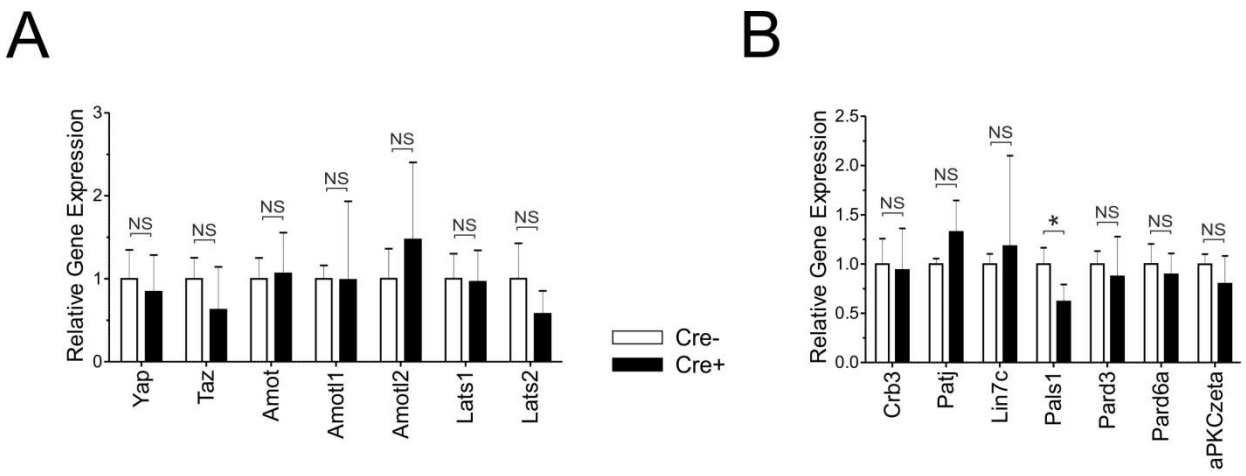

Fig. SF5: *Relative expression levels of target genes of the Hippo pathway and apical polarity genes.*

A: Real-time PCR analysis revealed no significant differences in expression of targets of the Hippo pathway in Pals1-deficient kidneys (Six2-Cre+) relative to controls (Six2-Cre-). **B:** In Pals1-deficient kidneys (Six2-Cre+) decreased gene expression of *Pals1* was confirmed. Expression of other polarity genes was not significantly altered. All data are shown as mean + SD of at least three independent experiments.

Suppl. Fig. SF6

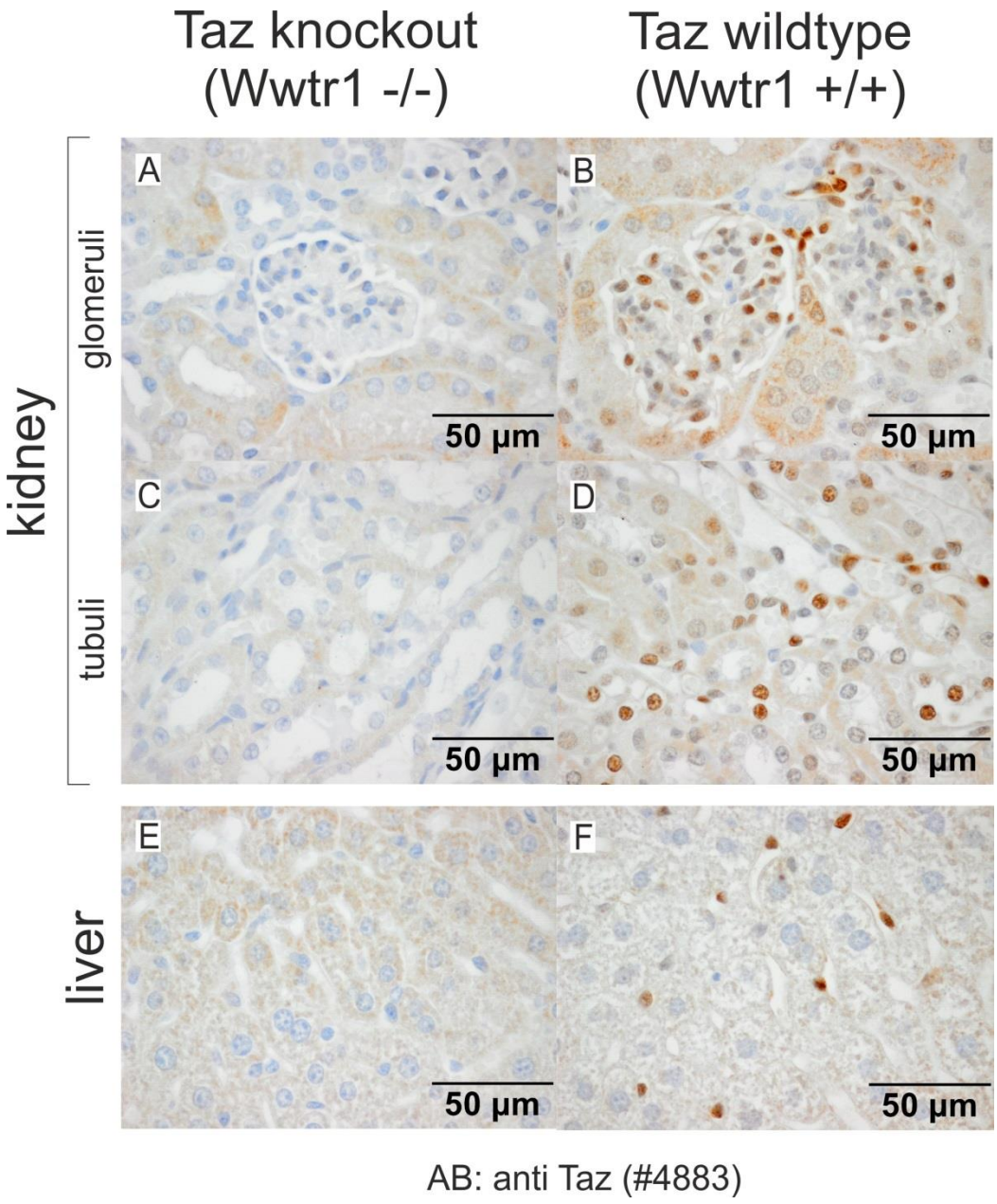

Fig. SF6: *Immunohistology staining using Taz$^{-/-}$ tissue.*

The validation of the anti-Taz antibody from Cell Signaling (#4883) on Taz$^{-/-}$ tissues (kindly provided by T. Benzing and B. Schermer), indicates a high preference of this antibody for Taz. This antibody has also been used by Gandhirajan et al (JBC 2016).[4]

Suppl. Fig. SF7

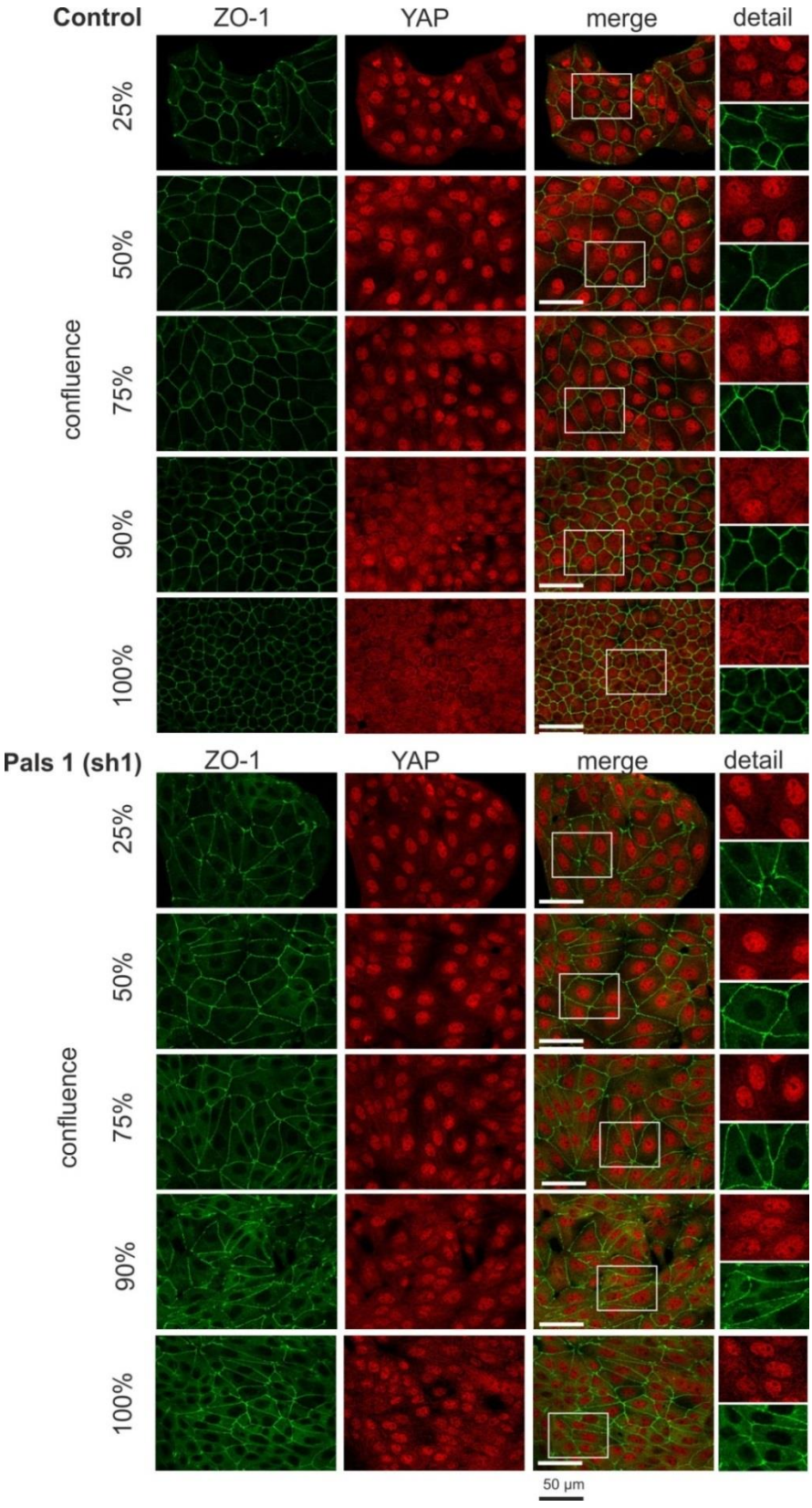

Fig. SF7: *Nuclear export of Yap is delayed in Pals1 KD MDCK cells.*

Immunostaining analysis of Yap (red) and the junctional marker ZO-1 (green) in control and Pals1 KD cells. Increasing confluence is associated with increasing export of Yap from the nuclei to the cytoplasm in control cells. In Pals1 KD cells (sh1), export of YAP from the nucleus is delayed. Even in almost confluent cells (90-100% confluence) YAP remains predominantly localized in the nuclear compartment. In comparison with the control, ZO-1 shows a more diffuse distribution, and significant amounts of the protein remain in the cytoplasm. Scale bars: 50 µm.

Suppl. Fig. SF8

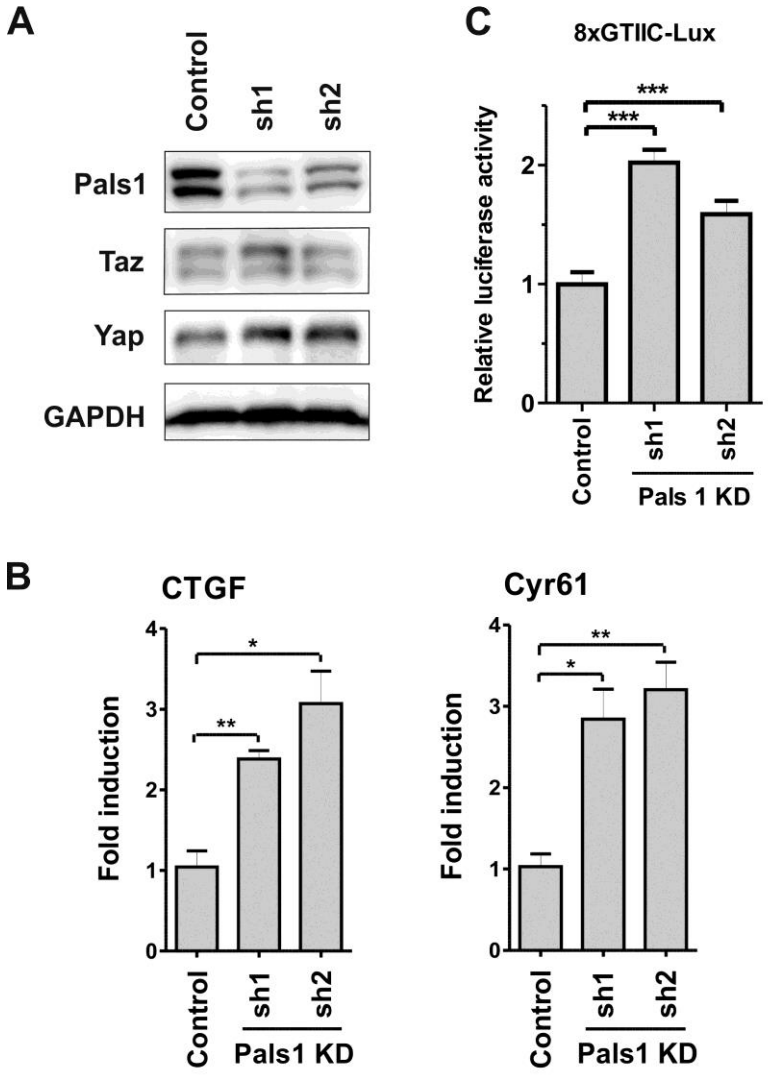

Suppl. Fig SF8: *Reduced Pals1 expression in HEK293T cells results in altered Hippo signaling.*

A: Knockdown of Pals1 in HEK293T cells (sh1 and sh2) has no influence on Taz and Yap expression. Actin served as loading control. **B:** Expression of the Hippo target genes *CTGF* and *CYR61* is increased in Pals1 KD cells (RT-PCR data are shown as mean + SD of at least three independent experiments). **C:** The results of the 8xGTIC-Lux reporter gene assay showed that Pals1 knockdown significantly enhances Yap/Taz-dependent transcriptional activity (data are presented as mean + SD and normalized to lane 1).

Suppl. Fig. SF9

A

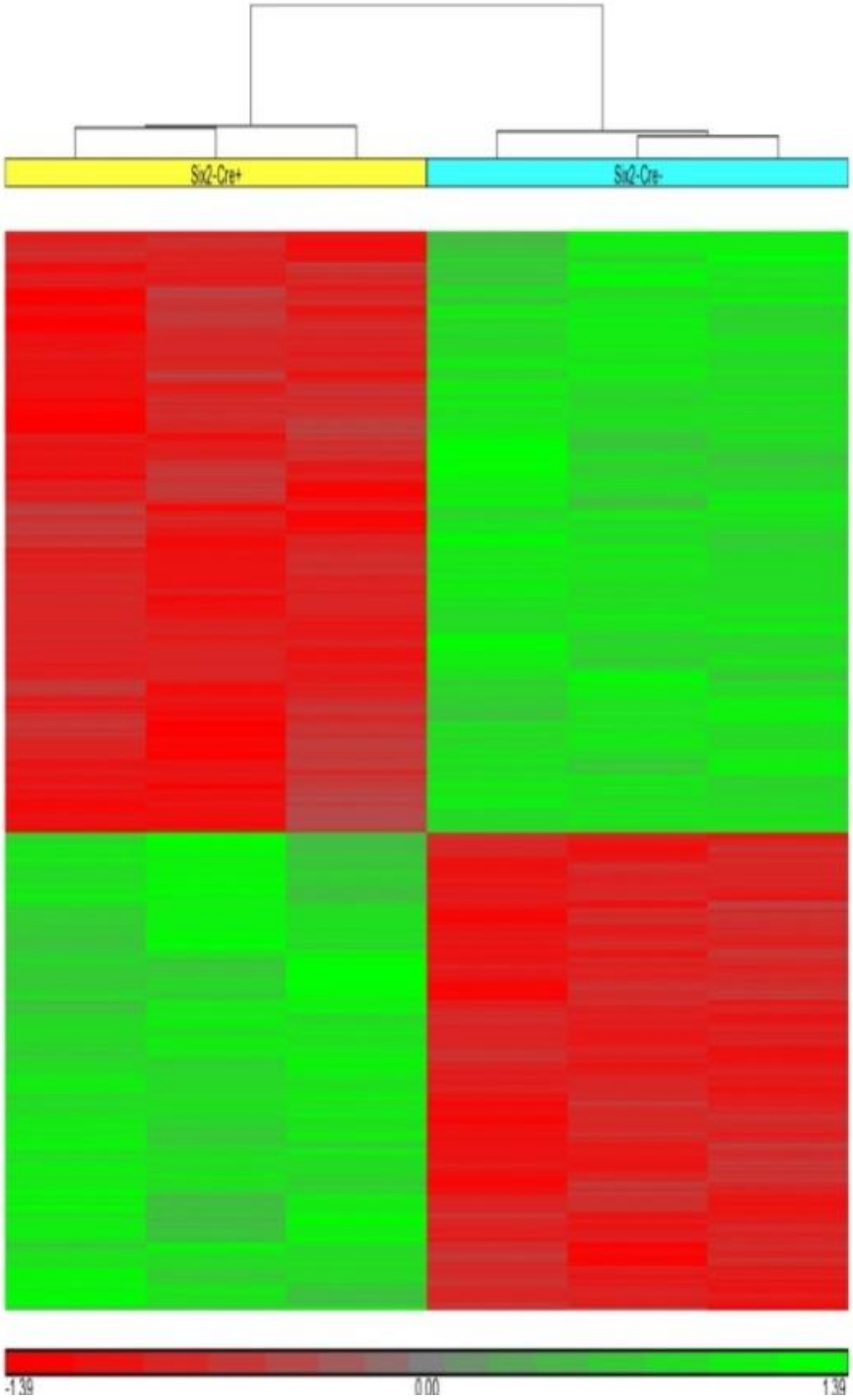

B

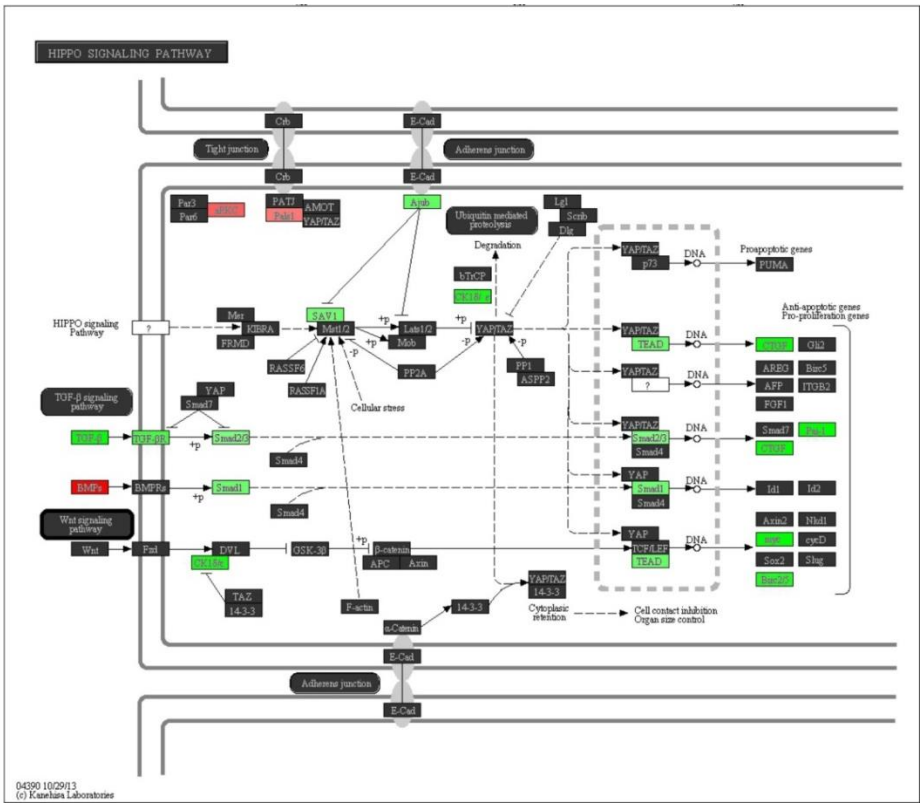

Suppl. Fig. SF9: *Gene expression analysis in Pals1-depleted mice versus littermate controls.*

Microarray experiments were performed to compare the gene expression profiles of Pals1-depleted Six2-Cre, Pals1$^{wt/fl}$ (Six2-Cre+) mice and their littermate controls Pals1$^{wt/fl}$ (Six2-Cre-). **A:** HEAT map showing the hierarchical clustering of differentially expressed genes. The data set (each N=3) was homogenous, allowing the different gene expression profiles to be compared. **B:** KEGG pathway diagram: Several target genes of the Hippo pathway, but also genes that respond to TGFβ signaling were up- (green) or downregulated (red) in Pals1-depleted kidneys.

Supplemental Tables

Suppl. Table ST1: Reduced *Pals1 expression results in an increased expression of renal injury marker genes.*

In Pals1-deficient kidneys (Six2-Cre+) renal injury marker genes are highly upregulated (selection). The complete list of differentially expressed genes is given in the suppl. data files SD2 and SD3.

Gene	Alias / Protein	Fold change	p-Value	Reference*
Havcr1	Kidney injury molecule -1 (Kim-1)	29.37	1.03 E-03	Fassett et al. 2011[5]
Lcn2	Lipocalin-2; Neutrophil gelatinase-associated lipocalin (Ngal)	12.98	1.16 E-05	Fassett et al. 2011[5]
Edn1	Endothelin 1 (Et-1)	8.21	9.01 E-06	Kohan & Barton, 2014[6]
C3	Complement component 3	7.46	5.76 E-04	Caliskan & Kiryluk 2014[7]
Serpine1	Serine/cysteine peptidase inhibitor, clade E, member 1 Plasminogen activator inhibitor type 1 (Pai-1)	8.60	3.56 E-04	Malgorzewicz et al., 2013[8]
Ltbp2	Latent transforming growth factor beta binding protein 2	8.67	5.92 E-03	Haase et al., 2014[9]
Gpnmb	Glycoprotein(transmembrane) Nmb (HGFIN, Osteoactivin)	8.74	5.33 E-04	Patel-Chamberlin et al., 2011[10] Pahl et al., 2010[11]
Mmp7	Matrix metallopeptidase 7 (Matrilysin)	7.81	1.01 E-04	Surendran et al., 2004[12]
Ccl2	CC-chemokine ligand 2; Monocyte chemoattractant protein-1 (Mcp-1)	8,93	2.56 E-04	Urbschat et al., 2011[13]
Tagln	Transgelin 1 (SM22)	7.17	2.24 E-03	Marshall et al., 2011[14] Ogawa et al., 2007[15]
Tagln2	Transgelin 2	8.93	2.56 E-04	Marshall et al., 2011[14] Ogawa et al., 2007[15]

*) References or reviews (with reference therein) that previously linked these genes to renal injury.

Suppl. Table ST2: Extended methods, details of antibodies and primer.

A: Antibodies used in the study

Antigen	**Species**	**Company**	**Cat #**	**Dilution Western Blot**	**Dilution IF, IHC**
Pals1/Mpp5	rabbit	ProteinTech	17710-1-AP	1:1000	1:50
α-Actinin-4	rabbit	Alexis	ALX-210-356	1:1000	
GAPDH	mouse	Covance Inc.	MMS-580S	1:2000	
Nephrin	guinea pig	Acris	BP5030	1:500	1:100
Podocin	rabbit	Sigma-Aldrich	P0372	1:1200	
Actin	rabbit	Sigma-Aldrich	A2066	1:1000	
E-Cadherin	mouse	BD Transduction	610182	-	1:100
ZO-1	mouse	Invitrogen	61-7300	-	1:50
Yap	rabbit	Cell signaling technology (CST)	XP #14074	1:1000	1:100
pYap S-127	rabbit	CST	#4911	1:1000	
Taz	rabbit	CST	#4883	1:1000	1:100
Aquaporin2 (AQP2)	rabbit	Sigma Aldich	SAB5200110		1:50
11-beta-Hydroxysteroid Dehydrogenase Type II (11beta HSD2)	sheep	Millipore	AB1296		1:100
Tamm-Horsefall Protein	mouse	Santa Cruz laboratories	sc-71022		1:50
Megalin	mouse	Acris	DM3613P		1:100
Alexa Fluor 594 Phalloidin	-	Invitrogen		-	1:200
DAPI	-	Roche		-	1:1000
HRP-conjugated secondary antibodies		Dianova			1:2500
Alexa coupled 2nd Abs for IF	-	Life technologies			1:1000
Rabbit serum	rabbit	Dianova	011-000-120		10% in Tris
Anti-rabbit IgG Alexa647	donkey	Life technologies	A31573		1:200
Anti-rabbit IgG Alexa568	donkey	Life technologies	A10042		1:200
Anti-mouse IgG Alexa488	donkey	Life technologies	A21202		1:200
Anti-sheep IgG Alexa568	donkey	Life technologies	A21099		1:200
Anti-rabbit Fab fragment	donkey	Jackson Immuno research	711-007-003		1:50

B: Primers used for SYBR Green RT-qPCR in mice.

Target	**Species**	**Direction**	**Sequence (5'-3')**
Amot	mouse	forward	CAGCCAGGGCAACACAGG
Amot	mouse	reverse	GACAGGTGAGCAGAGTGGTC
AmotL1	mouse	forward	GGGAAAAGCGTAGAGGACCC
AmotL1	mouse	reverse	TTGAGTGAGGGTTTCCGTGG
AmotL2	mouse	forward	GGACACCCTCTCTGGACTCT
AmotL2	mouse	reverse	CATGCACCAAGGCATCACTG
Birc2	mouse	forward	TGAGCAGCTGTTGTCCACTT
Birc2	mouse	reverse	GAACCGTCTGTCTCACCAGG
Birc5	mouse	forward	GAACCCGATGACAACCCGAT
Birc5	mouse	reverse	TGGTCTCCTTTGCAATTTTGTTCT
Ccl2	mouse	forward	AGCTGTAGTTTTTGTCACCAAGC
Ccl2	mouse	reverse	TGCTTGAGGTGGTTGTGGAA
Crb3	mouse	forward	GAGCCTAACAGCACCGGAC
Crb3	mouse	reverse	CCCGAAGTTTTCGCATGAGC
Ctgf	mouse	forward	GTGTGCACTGCCAAAGATGG
Ctgf	mouse	reverse	ATTTCCCAGGCAGCTTGACC
Cyr61	mouse	forward	CACTGAAGAGGCTTCCTGTCTT
Cyr61	mouse	reverse	GATCCGGGTCTCTTTCACCA
GAPDH	mouse	forward	TGGCCTTCCGTGTTCCTACC
GAPDH	mouse	reverse	GGTCCTCAGTGTAGCCCAAGATG
Havcr1	mouse	forward	GCATCTCTAAGCGTGGTTGC
Havcr1	mouse	reverse	TGCAGCTGGAAGAACCAACA
Lats1	mouse	forward	TGAGAAGAGTGCGGACAGTG
Lats1	mouse	reverse	TGAGATAATCCAACCCGCATCAT
Lats2	mouse	forward	GCAAGAGATTCGAGAGGGGC
Lats2	mouse	reverse	CCATCTCCTGGTCACATCCC
Lcn2	mouse	forward	ACGGACTACAACCAGTTCGC
Lcn2	mouse	reverse	AATGCATTGGTCGGTGGGG
Lin7c	mouse	forward	AATGGAGTGAGTGTTGAAGGGG
Lin7c	mouse	reverse	TACAATCACTGGCGTGGAGG
Pals1/Mpp5	mouse	forward	TCAGGCACTTTTACTGGCCC
Pals1/Mpp5	mouse	reverse	AACTGTGGCACCCAATGGAA

Pard3	mouse	forward	GATGTAACGAGCTGCGGTCT
Pard3	mouse	reverse	ACCCATTATCCTGCTCAGTGC
Pard6a	mouse	forward	CAGAAACGGGCAGAAGGTGA
Pard6a	mouse	reverse	TGAACCATGTTTGTGCAGCC
Patj	mouse	forward	TATCCTGCAGGTTGTGGCAG
Patj	mouse	reverse	TTCCAGGGTCTCGCCATTTC
Prkcz	mouse	forward	TCCGTCTGAAGGCGCAC
Prkcz	mouse	reverse	ACAAGGGTCACCTTCACTGTC
Tagln	mouse	forward	TTATGAAGAAAGCCCAGGAGCA
Tagln	mouse	reverse	TTTGTGAGGCAGGCTAAGCA
Taz/Wwtr1	mouse	forward	CTGAGTCCACAGAACCACCC
Taz/Wwtr1	mouse	reverse	GGGCCCTCCATTGAGGAAAG
Yap1	mouse	forward	CCCTCGTTTTGCCATGAACC
Yap1	mouse	reverse	TGCTCCAGTGTAGGCAACTG

C: Primers used for SYBR Green RT-qPCR in MDCK cell lines.

Target	**Species**	**Direction**	**Sequence (5'-3')**
Birc2	dog/MDCK	forward	GGCCGCGATTAACAGAGGG
Birc2	dog/MDCK	reverse	CCTTGCCTGTTTTGGCATGT
Cyr61	dog/MDCK	forward	CTGGTCAAAGTTACCGGCCA
Cyr61	dog/MDCK	reverse	CCGTTCCAAAAACTGGGAGG
Pai-1 /Serpine 1	dog/MDCK	forward	AACCTGGCGGACTTCTCAAG
Pai-1 /Serpine 1	dog/MDCK	reverse	ACTGTTCCTGTGGGGTTGTG

References

1. Kriz W, Hähnel B, Hosser H, Rösener S, Waldherr R. Structural analysis of how podocytes detach from the glomerular basement membrane under hypertrophic stress. *Front Endocrinol (Lausanne)*. 2014;5:207. doi:10.3389/fendo.2014.00207.

2. Kao RM, Vasilyev a., Miyawaki a., Drummond I a., McMahon a. P. Invasion of Distal Nephron Precursors Associates with Tubular Interconnection during Nephrogenesis. *J Am Soc Nephrol*. 2012;23(10):1682-1690. doi:10.1681/ASN.2012030283.

3. Muzumdar MD, Tasic B, Miyamichi K, Li L, Luo L. A global double-fluorescent Cre reporter mouse. *Genesis*. 2007;45(9):593-605. doi:10.1002/dvg.20335.

4. Gandhirajan RK, Jain M, Walla B, et al. Cysteine S-glutathionylation promotes stability and activation of the Hippo downstream effector transcriptional Co-activator with PDZ-binding motif (TAZ). *J Biol Chem*. 2016;291(22):11596-11607. doi:10.1074/jbc.M115.712539.

5. Fassett RG, Venuthurupalli SK, Gobe GC, Coombes JS, Cooper MA, Hoy WE. Biomarkers in chronic kidney disease: a review. *Kidney Int*. 2011;80(8):806-821. doi:10.1038/ki.2011.198.

6. Kohan DE, Barton M. Endothelin and endothelin antagonists in chronic kidney disease. *Kidney Int*. 2014;86(5):896-904. doi:10.1038/ki.2014.143.

7. Caliskan Y, Kiryluk K. Novel Biomarkers in Glomerular Disease. *Adv Chronic Kidney Dis*. 2014;21(2):205-216. doi:10.1053/j.ackd.2013.12.002.

8. Małgorzewicz S, Skrzypczak-Jankun E, Jankun J. Plasminogen activator inhibitor-1 in kidney pathology (Review). *Int J Mol Med*. 2013;31(3):503-510. doi:10.3892/ijmm.2013.1234.

9. Haase M, Bellomo R, Albert C, et al. The identification of three novel biomarkers of major adverse kidney events. *Biomark Med*. 2014;8(10):1207-1217. doi:10.2217/bmm.14.90.

10. Patel-Chamberlin M, Wang Y, Satirapoj B, et al. Hematopoietic growth factor inducible neurokinin-1 (Gpnmb/Osteoactivin) is a biomarker of progressive renal injury across species. *Kidney Int*. 2011;79(10):1138-1148. doi:10.1038/ki.2011.28.

11. Pahl M V., Vaziri ND, Yuan J, Adler SG. Upregulation of Monocyte/Macrophage HGFIN (Gpnmb/Osteoactivin) Expression in End-Stage Renal Disease. *Clin J Am Soc Nephrol*. 2010;5(1):56-61. doi:10.2215/CJN.03390509.

12. Surendran K, Simon TC, Liapis H, McGuire JK. Matrilysin (MMP-7) expression in renal tubular damage: Association with Wnt4. *Kidney Int*. 2004;65(6):2212-2222. doi:10.1111/j.1523-1755.2004.00641.x.

13. Urbschat A, Obermüller N, Haferkamp A. Biomarkers of kidney injury. *Biomarkers*. 2011;16 Suppl 1:S22-30. doi:10.3109/1354750X.2011.587129.

14. Marshall CB, Krofft RD, Blonski MJ, et al. Role of smooth muscle protein SM22α in glomerular epithelial cell injury. *Am J Physiol Renal Physiol*. 2011;300(4):F1026-42. doi:10.1152/ajprenal.00187.2010.

15. Ogawa A, Sakatsume M, Wang X, et al. SM22α: The Novel Phenotype Marker of Injured Glomerular Epithelial Cells in Anti-Glomerular Basement Membrane Nephritis. *Nephron Exp Nephrol*. 2007;106(3):e77-e87. doi:10.1159/000103020.